THE JOURNAL OF BIOLOGICAL CHEMISTRY VOL. 286, NO. 26, pp. 22875–22885, July 1, 2011

In Vitro Motility of Liver Connexin Vesicles along Microtubules Utilizes Kinesin Motors*[S]

Received for publication, January 8, 2011, and in revised form, April 17, 2011 Published, JBC Papers in Press, May 2, 2011, DOI 10.1074/jbc.M111.219709

Alfredo G. Fort[‡], John W. Murray[§], Nadine Dandachi[‡], Michael W. Davidson[¶], Rolf Dermietzel[‖], Allan W. Wolkoff[§], and David C. Spray[‡1]

From the [‡]Dominick P. Purpura Department of Neuroscience and [§]Department of Anatomy and Structural Biology, Albert Einstein College of Medicine, Bronx, New York 10461, the [¶]National High Magnetic Field Laboratory and Department of Biological Science, The Florida State University, Tallahassee, Florida 32310, and the [‖]Neuroanatomy and Molecular Brain Research, Ruhr University, 44801 Bochum, Germany

Trafficking of the proteins that form gap junctions (connexins) from the site of synthesis to the junctional domain appears to require cytoskeletal delivery mechanisms. Although many cell types exhibit specific delivery of connexins to polarized cell sites, such as connexin32 (Cx32) gap junctions specifically localized to basolateral membrane domains of hepatocytes, the precise roles of actin- and tubulin-based systems remain unclear. We have observed fluorescently tagged Cx32 trafficking linearly at speeds averaging 0.25 μm/s in a polarized hepatocyte cell line (WIF-B9), which is abolished by 50 μM of the microtubule-disrupting agent nocodazole. To explore the involvement of cytoskeletal components in the delivery of connexins, we have used a preparation of isolated Cx32-containing vesicles from rat hepatocytes and assayed their ATP-driven motility along stabilized rhodamine-labeled microtubules *in vitro*. These assays revealed the presence of Cx32 and kinesin motor proteins in the same vesicles. The addition of 50 μM ATP stimulated vesicle motility along linear microtubule tracks with velocities of 0.4–0.5 μm/s, which was inhibited with 1 mM of the kinesin inhibitor AMP-PNP (adenylyl-imidodiphosphate) and by anti-kinesin antibody but only minimally affected by 5 μM vanadate, a dynein inhibitor, or by anti-dynein antibody. These studies provide evidence that Cx32 can be transported intracellularly along microtubules and presumably to junctional domains in cells and highlight an important role of kinesin motor proteins in microtubule-dependent motility of Cx32.

Gap junction channels form direct intercellular passageways that allow the exchange of ions and second messenger molecules between cells, thereby spreading signals and unifying cellular responses within a tissue. Gap junctions are formed by the connexin family of proteins that are co-translationally inserted into endoplasmic reticulum membranes (1) and assembled into hexameric connexons or hemichannels within the endoplasmic reticulum or Golgi compartments depending on connexin, cell type, or both (2–6). Connexins are tetra-spanning transmembrane proteins with both termini (N termini and C termini) facing the cytoplasm. This conformation results in two extracellular loops required for connexon docking and one cytoplasmic loop.

Knowing the mechanisms of delivery is crucial to understanding connexin regulation because insertion into the plasma membrane is a prerequisite to connexin function. The route of delivery of connexons from the trans-Golgi to the surface membrane has been the subject of many studies, most recently focusing on exogenously expressed connexins with carboxyl-terminally tagged fluorescent proteins. These studies have indicated that the vesicular structures in which connexins are delivered to the surface occur in a variety of sizes and are motile. Moreover, although delivery appears to be facilitated by microtubules, intact cytoskeleton is not absolutely required for trafficking, as evidenced by the variable effects reported for microtubule-disrupting agents (7–15). Nevertheless, intracellular transport of connexins with fluorescent tags, exogenously expressed in cells, appears to be following linear and oriented movements, consistent with targeted delivery via cytoskeletal elements (8). However, the role that microtubules and microtubule motors play in delivery of connexin proteins has not being studied in detail and remains undefined. In this study, we have made similar observations with a variant GFP-tagged Cx32[2] construct exogenously expressed in a polarized hepatocyte cell model and furthermore observed that microtubule disruption abolishes particle motility. We, therefore, hypothesize that microtubule and microtubule motors play a role in delivery of connexins, more specifically Cx32, to the plasma membrane.

To gain insight into the fundamental mechanisms involved in gap junction trafficking to the surface membrane, we have explored microtubule involvement in a simplified system in which *in vitro* polymerized-microtubules were studded with Cx32-containing vesicles isolated from rat liver, a rich source of this gap junction protein, which are immunofluorescently labeled. When stimulated by the addition of ATP, a fraction of these vesicles moved along the microtubules, with velocities similar to those seen in exogenously expressing cells. Moreover, based on findings that certain motor proteins are present in these vesicles as well as the inhibition of vesicular motility by kinesin motor protein inhibitors, we conclude that kinesin

* This work was supported, in whole or in part, by National Institutes of Health Grant DK41918 (to D. C. S. and A. W. W.).

[S] The on-line version of this article (available at http://www.jbc.org) contains supplemental Figs. 1 and 2 and Movies 1–5.

[1] To whom correspondence should be addressed: 1300 Morris Park Ave., Kennedy 830, Bronx, NY 10461. Tel.: 718-430-2537; Fax: 718-430-8594; E-mail: david.spray@einstein.yu.edu.

[2] The abbreviations used are: Cx32, connexin32; AMP-PNP, adenylyl-imidodiphosphate.

plays a major role in trafficking of the connexin vesicles along the microtubules. We interpret these results as indicative of microtubule and microtubule-kinesin motor-dependent trafficking of Cx32, which presumably occurs in cells expressing Cx32, such as hepatocytes in liver and in myelinating glia (Schwann cells and oligodendrocytes) in the peripheral and central nervous system, and highlighting another checkpoint in the regulation of Cx32 function.

EXPERIMENTAL PROCEDURES

Unless otherwise noted, all reagents were obtained from Sigma-Aldrich.

Cx32-mEmerald Construct—The enhanced GFP (EGFP) derivative Emerald (emGFP, EGFP + S72A/N149K/M153T,I167T, Invitrogen) was converted to the A206K variant using the Lightning mutagenesis kit (Agilent Technologies, Santa Clara, CA), and the resulting cDNA was amplified with a 5′ primer encoding an AgeI site and a 3′ primer encoding a NotI site. The purified and digested PCR products were ligated into a similarly digested EGFP-N1 cloning vector (Clontech) operating under CMV control. To prepare the Cx32 fusion, a CMV-Clontech vector containing enhanced YFP (EYFP) fused to human β-1 connexin32 with a 7-amino acid linker (ADPPVAT) and the mEmerald-N1 cloning vector were digested with BamHI and NotI. After purification, the PCR products were ligated to produce Cx32-7-mEmerald.

Vector DNA for transfection was prepared using the plasmid maxi kit (Qiagen, Valencia, CA). To ensure proper localization, Cx32-7-mEmerald was characterized by transfection in HeLa cells (CCL2 line; ATCC, Manassas, VA) using Effectene (Qiagen) and ~1 μg of vector. Transfected cells were grown on coverslips in DMEM/F12, fixed after 48 h, and mounted with Gelvatol. Epifluorescence images were captured with a Nikon 80i microscope using wide field illumination and a FITC filter set, showing proper localization in gap junction plaques using Cx32-7-EGFP as a control (not shown).

Culture and Transfection of WIF-B9 Cells—WIF-B9 cells, a hepatoma-human fibroblast fusion cell line that forms functional bile canaliculi, were kindly obtained at passage p4 from Dr. Anne Muesch (Department of Developmental and Molecular Biology, Albert Einstein College of Medicine, Bronx, NY). Cells were maintained in culture in a humid environment with 5% CO_2 at 37 °C using F12 medium supplemented with sodium bicarbonate, 1% GlutaMAX, 5% FBS, 1% penicillin/streptomycin, 0.2% Fungizone. Freshly split cells (within 2 h after splitting) were transfected with 2 μg of plasmid containing human full-length Cx32-mEmerald using Lipofectamine LTX + Plus reagent (Invitrogen). Briefly, cells were resuspended using serum-free Opti-MEM (Invitrogen) medium instead of regular growth medium and plated in culture dishes with glass bottoms for imaging (MatTek Corp., Ashland, MA; P35G-1.5-14-C), and then DNA-Lipofectamine complexes were added to the culture. Cells were incubated at 37 °C for 4 h, and then medium was changed, and cells were assayed for protein expression and imaging 48 h later. WIF-B9 cells were placed in a 10-min 10 °C preincubation and treated at 37 °C with 50 μM nocodazole for 1.5 h prior to imaging at 28 °C to determine the effects of microtubule disruption Cx32-mEmerald vesicle motility.

Antibodies—Anti-Cx32 mouse monoclonal (C6344) and rabbit polyclonal antibodies (generated against cytoplasmic loop and C termini cytoplasmic domains of Cx32) were obtained from Sigma (polyclonal antibodies C3595 and C3470, respectively). Kinesin (90 and 120 KDa) heavy chain antibodies generated against the conserved globular N-terminal head were purchased from Cytoskeleton Inc. (Denver, CO; and rabbit polyclonal AKIN01 and mouse monoclonal AKIN02/SUK4), and a mouse monoclonal antibody was purchased from Millipore Corp. (Billerica, MA; clone H2: MAB1614). Mouse monoclonal anti-kinesin light chain antibody was purchased from Millipore (MAB1616). Other antibodies used include mouse monoclonal anti-GAPDH (Sigma, G8795), anti-Cx26 goat polyclonal antibody (Abcam, Cambridge, UK; ab59020), anti-Lamp1 mouse monoclonal antibody (Abcam, ab13523), mouse monoclonal anti-dynein light chain (Millipore, MAB1076), mouse monoclonal anti-Rab4 (BD Biosciences; 610888), rabbit monoclonal anti-EEA1 (Cell Signaling Technology, Inc., Danvers, MA; 2411S), goat polyclonal anti-clathrin (Santa Cruz Biotechnology Inc., Santa Cruz, CA; sc-6579), mouse monoclonal anti-synaptophysin (Sigma S5768), and mouse monoclonal anti-β/α-tubulin (Sigma, T6074 and T0198, respectively). Secondary polyclonal antibodies Alexa Fluor 488/594-conjugated goat anti-mouse or -rabbit from Molecular Probes (Invitrogen) were used for indirect immunofluorescence (488 nm mouse/rabbit, A-11001/A-11008; 594 nm mus/rab, A-11005/A-11012, respectively; and Alexa Fluor 594-conjugated rabbit anti-goat, A-21223). For indirect immunodetection of Western blotted proteins, we used HRP-conjugated goat anti-mouse and -rabbit secondary antibodies (Santa Cruz Biotechnology, sc-2005/sc-2004, respectively).

Isolation of Cytoplasmic Membrane Vesicles—The protocol used to isolate vesicles from liver has been published (16). Briefly, Sprague-Dawley rats were i.v. injected with 50 μg of Texas Red-labeled asialoorosomucoid for 5 min, to label early endosomes, and then the animals were perfused with 30 ml of ice-cold PBS. Livers were removed from the animal, washed with PBS and then MEPS (35 mM Pipes, pH 7.4, 5 mM EGTA, 5 mM $MgSO_4$, 0.2 M sucrose), diced with a razor blade, and added to 15 ml of MEPS plus protease inhibitor mixture (Sigma P8340). The mix was homogenized with 20 strokes using a loose Dounce (Wheaton Scientific, Millville, NJ), and the resulting lysate was centrifuged at 3,000 rpm (1,811 × *g*) for 10 min at 4 °C. The postnuclear supernatant was then removed and supplemented with DTT and protease inhibitor mixture. The postnuclear supernatant was applied to a Sephacryl S200 gel filtration column (Amersham Biosciences, Uppsala, Sweden) equilibrated in MEPS, and the void volume containing the endosomes was applied to the bottom of a 0.25/1.2/1.4 M discontinuous sucrose gradient and ultracentrifuged for 135 min at 39,000 rpm, at 4 °C. Approximately 1.2 ml was collected from the 0.25/1.2 M interface and aliquoted for storage at −80 °C or liquid nitrogen. Samples were measured for protein content using the BCA kit from Pierce (Thermo Fisher Scientific). For immunostaining of vesicles, endosome isolation was obtained from rats as described above but without the injection of labeled asialoorosomucoid.

Western Blotting—Lysate collection for tissues and vesicles was similar. For tissues, mice were deeply sedated and operated to expose the heart and liver and then perfused with cold PBS through the left ventricle until the liver and heart were blanched. The tissues were then removed and placed in ice-cold PBS for two rounds of gentle washing and then transferred to a 60-mm dish with 5 ml of Lysis Buffer (1% Triton X-100, 50 mM Tris-HCl at pH 7.4, 300 mM NaCl, 5 mM EDTA). The tissues were minced with a sharp, clean blade and passed through a cloth mesh, and the collection was then spun at 10,000 × *g* for 15 min at 4 °C. Supernatant was removed and placed in a new Eppendorf tube, and a 10-μl sample was used for protein quantification using a BCA kit (Pierce 23225). The remaining was supplemented with protease inhibitor mixture (Sigma, P8340) and 1 mM PMSF. A 100-μl sample was saved for whole lysate Western blotting; the remainder was either used immediately or separated into aliquots for storage at −80 °C. It should be noted that these samples were all normalized with respect to total protein, and thus, band intensity directly reflects the relative amount of each protein in the total lysate.

Samples were processed by electrophoresis in 10% Tris-based SDS-denaturing polyacrylamide gels using 55-V and 35-mA currents for 1.5–2 h and then trans-blotted onto a nitrocellulose membrane at 300 mA (~80 V) for 1 h in a 4 °C cold room. The membrane was left overnight with 3% skim milk in TBS (20 mM Tris-HCl, pH 7.4, 150 mM NaCl) complemented with 0.05% Tween 20 detergent (Western blot blocking solution) followed by incubation with dilution of 1:500–1000 of primary antibody in Western blot blocking solution overnight at 4 °C or 2 h at room temperature. After incubation, the membrane was washed 3 × 5 min in Western blot wash solution (TBS with 0.05% Tween 20) and then incubated with 1:5000–20,000 HRP-conjugated secondary antibody in Western blot blocking solution for 1 h at room temperature. Membrane was washed 5 × 5 min, and HRP signal was developed with the Amersham Biosciences ECL kit (GE Healthcare Ltd.). The membrane was then photoprinted onto a Kodak film (Perkin-Elmer Life Sciences) in a dark room. It should be noted that a band was observed when using primary monoclonal antibodies in both tissue and vesicle samples, which was determined to originate from the anti-mouse secondary antibody (see supplemental Fig. 1 and its legend).

Immunoprecipitation—An antibody-Sepharose bead complex was prepared at 4 °C 16 h in advance, where 1 μg of polyclonal Cx32 or 2 μg of monoclonal kinesin antibody was preincubated with 50 μl of a 50% slurry of protein A/G-Sepharose beads (Amersham Biosciences) and 500 μl of Lysis Buffer. The mix was spun at 3,000 × *g* for 10 min at 4 °C, and the supernatant containing unbound antibody was removed. Separately, liver lysate was dissolved in Lysis Buffer until a 1 mg/ml concentration was obtained, and then the lysate was precleared by adding 40 μl of a 50% slurry of protein A/G-Sepharose beads and rotated at 4 °C for 1 h. The tubes were then spun at 3,000 × *g* for 10 min at 4 °C to precipitate the beads. Usually, this was performed two times. 500 μl of supernatant was then carefully removed onto the tube containing the antibody-bead mix, which had been supplemented with 10 μl of 10% bovine serum albumin (BSA) to block unspecific binding to the complex. The lysate-antibody-bead mix was then left rotating at 4 °C for 4 h. The samples were centrifuged at 5,000 × *g* for 15 min at 4 °C. The supernatant was removed. The beads were then washed with 1 ml of Wash Buffer (0.1% Triton X-100, 50 mM Tris-HCl, pH 7.4, 300 mM NaCl, 5 mM EDTA), gently resuspended by tapping the Eppendorf tube, and spun once again. The washes were repeated twice. In the final step, all the supernatant was removed, and denaturing Loading Buffer was added to proceed with Western blotting, as above.

Micro-chambers—The construction of the micro-chambers for microtubule and vesicle motility experiments was minimally modified from Murray *et al.* (17). Using a commercial (Toyo) glass cutter, a plain glass microscope slide was cut transversely to a measure of 1.5 × 0.7 cm. The piece was washed once or twice in ethanol and then in distilled water to remove dust and grease and left to air-dry. Briefly, a 50-ml Falcon conical tube was cut in half around the 30-ml mark. The piece with the lid was inverted and filled with DEAE-dextran (final 20 μg/ml; from 150× stock) in distilled water. The other half was placed on a Styrofoam holder and filled with ethanol (70%). The same procedure was applied to an oblong cover glass (22 × 40 mm No. 1, Gold Seal, Thermo Scientific). After light air-drying, the cover glass was dipped completely into the DEAE-dextran cuvette 8–10 times, then rinsed thoroughly with distilled water using a nozzle. The cover glass was air-dried again and then placed on a clean surface. Two strips of double-sided Scotch adhesive tape were cut, about 1.2 × 0.4 cm, and placed on the cover glass parallel to its long axis, leaving a 0.5–1-cm space. Finally, the cut glass slide piece was lowered on top perpendicular to the Scotch tape and pressed firmly to seal the adhesive tape, providing a micro-chamber with a working volume of 7–15 μl.

Immunostaining of Vesicles in Micro-chambers—The micro-chamber surface was washed twice with 100 μl of "Assay Buffer" (35 mM Pipes, 5 mM $MgCl_2$, 1 mM EGTA, 0.5 mM EDTA, 4 mM DTT, 20 μM Taxol, 2 mg/ml BSA, pH 7.4) by adding it in one end of the opening and gently absorbing the liquid at the other end with a folded KimWipe tissue. Vesicles were diluted into Assay Buffer (to a final concentration of 2 mg/ml), and 4 μl was added to the chamber and incubated at room temperature for 10 min in a humid chamber. The unbound vesicles were rinsed away with 3 × 15-μl washes of Block Buffer (Assay Buffer + 5 mg/ml casein) and then incubated with 1:100–500 diluted primary antibody. Block Buffer was added and incubated for 5 min at room temperature in a humid chamber. This was followed by 3 × 15-μl washes with Block Buffer, and 1:500–1000 diluted secondary antibody added for 5 min at room temperature in a humid chamber. The last wash of 3 × 15 μl was left with Antibleach Buffer (Assay Buffer supplemented with 10 mM glucose, 52 units/ml catalase or horseradish peroxidase, and 26 units/ml glucose oxidase). The micro-chamber was then sealed with nail polish on both sides to avoid evaporation.

Fluorescent Microtubules—Polymerized microtubules were constructed as previously published (16). Unlabeled tubulin (Cytoskeleton Inc., TL238, 250 g) was dissolved in 25 μl of Buffer 1 (80 mM Pipes-K_2, 1 mM EGTA, 1 mM $MgCl_2$, 1 mM GTP, and 3% glycerol). 12 μl of unlabeled tubulin was added to

anhydrous rhodamine-labeled tubulin (Cytoskeleton Inc., TL331M, 20 μg), and centrifuged for 5 min at 14,000 rpm in a 4 °C cold centrifuge. 6 μl of unlabeled/labeled tubulin solution (11.7 μg/μl) was mixed with an additional 4 μl of unlabeled tubulin to a total of 10 μl. 7 μl of 37 °C warm Buffer 1 was added to 10 μl of the tubulin mix. The mixture was warmed to 37 °C for 8–15 min until the desired polymerization was reached (several tubes were made to determine the ideal microtubule length). The microtubules were stabilized by adding 190 μl of warm Buffer 1 supplemented with 20 μM Paclitaxel (Taxol) (Sigma, T7402). Centrifugation was then performed in a Beckman Airfuge apparatus (Beckman Coulter, Inc) at 15 p.s.i. for 5 min. The pellet was resuspended in 100 μl of Buffer 1 + 20 μM Paclitaxel. This preparation was used within 2 weeks and maintained at room temperature, wrapped in aluminum foil. A dilution of 1/50 was used to coat micro-chambers with microtubules.

Vesicle Motility—Experiments were performed following a previously published protocol (16). Diluted microtubules (1/50) in Buffer 1 supplemented with 20 μM Paclitaxel were added to a micro-chamber in 3 × 15-μl perfusions, with the last volume left in place for 3 min at room temperature. The micro-chamber was then washed three times with 12 μl of Buffer 1 without glycerol but with 10 μM Paclitaxel added and then three times with 12 μl of PMEE Buffer (35 mM Pipes-K_2, pH 7.4, 5 mM $MgCl_2$, 1 mM EGTA, 0.5 mM EDTA, 10 μM Paclitaxel, 4 mM DTT and 2 mg/ml BSA) supplemented with 5 mg/ml casein. The chamber was then washed three times with 12 μl of PMEE Buffer. Aliquots of vesicles were perfused into the microtubule-coated chambers 3 × 4 μl, and the last was maintained for 10 min followed by washing with PMEE Buffer. Chambers were then perfused with diluted primary antibodies in PMEE Buffer containing 5 mg/ml casein and without DTT, for 6 min at room temperature and then blocked with PMEE Buffer with casein and without DTT and perfused with diluted secondary antibody for 5 min. The secondary antibody was washed twice with PMEE Buffer supplemented with 10 mM glucose, 2% glucose oxidase, 2 μg/ml horseradish peroxidase, and 2 mg/ml vitamin C. The chamber was refrigerated in an ice box until use (no more than 2 h). Anti-motor antibodies were incubated after secondary antibody wash for 6 min at room temperature at 1:50 dilutions. When anti-motor antibodies were used, a different host primary antibody was chosen against Cx32. For motility imaging, 20 μl of PMEE Buffer freshly supplemented with 50 μM ATP was perfused through the chamber and imaged under epifluorescent microscopy in a 37 °C chamber.

Imaging and Data Analysis—Time-lapse microscopy of Cx32-transfected WIF-B9 cells were performed on a Zeiss LSM 510 Meta microscope (Carl Zeiss, Inc., Thornwood, NY) with appropriate filters for 488 nm excitation and band-pass filter 505–550 nm for emission capture. Dishes containing transfected cells were placed in conditioned chambers at 28 °C and imaged no longer than 30 min. Time-lapse images were obtained at 1–5-s intervals for 5–15 min using a 63× oil immersion objective with 1.4 numerical aperture (NA) and 2× zoom, keeping the 100 milliwatt 488 nm laser power between 1 and 3%, and high scan speed to avoid cell damage. Three z-plane slices, of 0.34- or 0.7-μm separation, were obtained for each time point to avoid losing vesicles that drifted from the plane of view; this resulted in xyzt dimensional stacks. Images were captured using the LSM software. Images were then analyzed using the ImageJ software (National Institutes of Health). Time-lapse microscopy of micro-chambers was performed with an Olympus 1 × 71 microscope in a conditioned chamber at 37 °C with a 60 × 1.4 NA objective and automated excitation and emission filter sets for fluorescence capture. Data were recorded with a CoolSNAP HQ cooled CCD (Photometrics, Roper Scientific, Tucson AZ) controlled by the MetaMorph software (Molecular Devices, Sunnyvale, CA).

To track Cx32-mEmerald vesicles, xyzt stacks were z-projected using the maximum pixel intensity value to obtain xyt stacks, and vesicles were tracked using the ImageJ manual tracking plugin. Distance displacements and calculated speed values were transferred to the Microsoft Excel program (Microsoft Corp., Redmond, WA) for further analysis. Vesicle speeds were calculated from the distance/time measurements, excluding stationary dwell times. In the text, average values are accompanied by standard error of the mean (S.E.) values, considering the different sizes of samples. To obtain time- and color-coded (*t*) images (see Fig. 1, *A* and *B*), we applied the Z-Code Stack plugin from ImageJ to the xyt stacks to spectrum-code all images in the stack, with red images at time 0, through green, to violet at the end of the recording. The time color-coded xyt stacks were then Z-projected using maximum intensity to compact all time points and obtain an xy time- and color-coded image. For immunolabeled Cx32-containing vesicles on fluorescent microtubules, images obtained were of one-plane, xyt format. Images were exported from MetaMorph and analyzed as mentioned above using ImageJ. In color-coded images, colored spots represent motile vesicles, whereas white spots represent near static vesicles.

Displacement graphs were obtained by obtaining the cumulative displacement for each particle at each time point (using the SUM function in Excel). Motility profile images in Fig. 4*B* were obtained for the time-lapsed dual-colored image in Fig. 4*A* by tracing a line over microtubules using ImageJ and then using the Stacks > Reslice function to obtain kymographs for motile vesicles.

Images of immunolabeled isolated vesicle samples performed in the micro-chambers were obtained, keeping exposure times for each channel the same in all images (2 s for 488 nm and 4 s for 561 nm), using an inverted Nikon TE2000 microscope (Nikon Instruments, Inc., Melville, NY) with a 60 × 1.4 NA objective, and captured using a monochrome SPOT RT CCD camera (Diagnostic Instruments, Inc., Sterling Heights, MI), with epifluorescence and proper filters for excitation and emission of the Alexa Fluor antibodies. Images were then processed in ImageJ for co-localization. We first obtained a qualitative analysis by measuring the area of co-localization between green and red signals, after thresholding images to bring background to zero. The co-localized area was then compared with the total area of signal from Cx32, to obtain the percentage of the co-localized area with respect to Cx32. For a quantitative analysis, we calculated Mander's coefficient (see Table 1, Footnote a) on images with a similar number of green/red pixels (18) using the ImageJ plugin provided by the Wright Cell Imaging

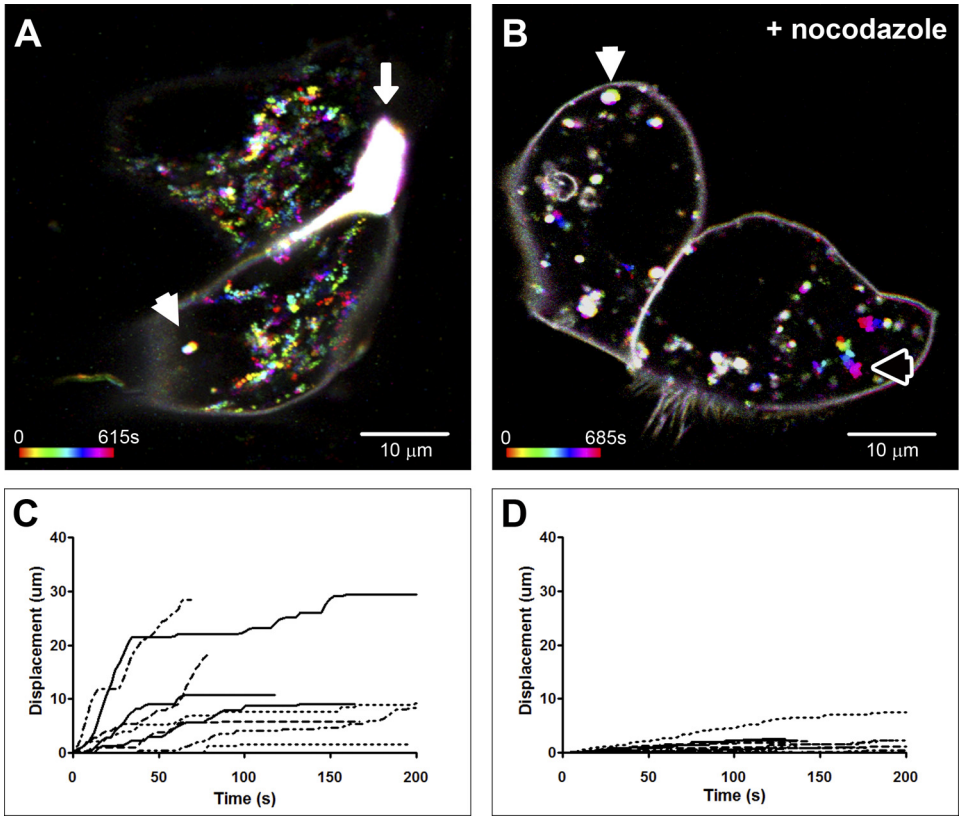

FIGURE 1. **Monomeric Emerald-tagged Cx32 exogenously expressed in WIF-B9 hepatocyte cell line traffics on microtubule-dependent pathways.** *A*, a time- and color-coded (see under "Experimental Procedures") 10-min live single confocal-plane image at 28 °C of two apposed WIF-B9 cells forming a gap junction plaque between them (*arrow*). The large number of multicolored trails, indicative of motile particles, demonstrates the ubiquitous motility of Cx32-mEmerald-containing vesicles. A few particles were stationary, resulting in a white spot (*arrowhead*). The *bottom left bar* shows color-coding corresponding to time points between 0 and 615 s. *B*, a color-coded 10-min recording of WIF-B9 cells after a 1.5-h incubation with 50 μM nocodazole at 37 °C. Particle motility was greatly decreased (*numerous white spots*). The *white* and *black arrowheads* highlight particles with little or moderate displacement, respectively. *C*, this graph shows the cumulative displacement of nine particles tracked in the control experiment (A). *D*, cumulative displacement graph of seven particles in the nocodazole-treated WIF-B9 cells. Note the lack of cumulative displacement with nocodazole in contrast to control. Average particle speed in control conditions was 0.246 ± 0.032 (S.E.) μm/s (n = 3; 16 vesicles); average nocodazole-treated vesicle speed was 0.066 ± 0.009 (S.E.) μm/s (n = 2; 17 vesicles).

Facility. Values closer to 1 signify high co-localization. Pearson's coefficients were also obtained and were similar to Mander's and are therefore not included here.

RESULTS

To establish the trafficking behavior of connexin-containing particles in cells, we transiently expressed mEmerald-tagged Cx32 in a hepatocyte cell line (WIF-B9) and performed time-lapse recordings in 37 °C-heated chambers using a Zeiss confocal microscope. In these experiments, we observed that within relatively short periods of time (~15 min), it was possible to clearly discern a large number of spheroid fluorescent particles that traveled in linear fashion throughout the cell (Fig. 1*A* and supplemental Movie 1). These vesicular particles were excluded from nuclei but otherwise traveled from one region in the cell to another at speeds averaging 0.25 ± 0.03 (S.E.) μm/s, typically with several stops (which we counted as dwell times) and starts along the way. Time- and color-coding the trajectories of these particles results in rainbow-colored trails that mark the passage and direction (Fig. 1*A*). To determine whether the behavior and speeds observed for these fluorescent vesicles were dependent on intact microtubules, we incubated cells with nocodazole (50 μM), a microtubule disruptor, for 1.5 h at 37 °C. This treatment resulted in a severe attenuation in the motility of fluorescent particles (Fig. 1*B* and supplemental Movie 2), with vesicle speeds averaging 0.07 ± 0.01 (S.E.) μm/s. This is reflected in the loss of long trails and the abundance of white signals, due to the superposition of low motility colored particles. These findings indicate that exogenously expressed Cx32-mEmerald particles are localized to vesicles whose trafficking in the cell is dependent on microtubules. To more closely examine the motility of these particles and the involvement of motor proteins in their trafficking, we isolated low density vesicles from rat liver homogenates (see under "Experimental Procedures").

Characterization of Motor Proteins within Endocytic Vesicles—We first confirmed the presence of both Cx32 and kinesin proteins in vesicles isolated from rat liver. Fig. 2 shows Western blots comparing protein profiles from liver tissue and isolated vesicles. An 81-KDa band positive for kinesin and three bands for Cx32 protein can be seen, where the lowest 28-KDa band corresponds to the monomeric form of Cx32 and the higher bands are presumed multimers. As controls, tubulin and glyceraldehyde-3-phosphate dehydrogenase (GAPDH) proteins are shown to be present in the tissue homogenates but not in the isolated vesicle samples. The lack of tubulin co-isolation with vesicles suggests that motor proteins present in this isolate

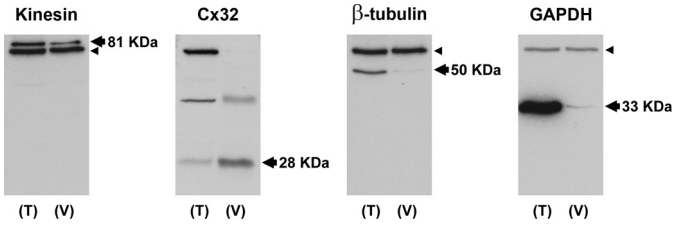

FIGURE 2. **Cx32 and kinesin are present in liver tissues and isolated vesicles.** Western blots of whole rat liver tissue (*T*) and isolated liver vesicles (*V*) after separation by SDS-PAGE are shown. All samples were normalized to 50 μg of total protein. Immunodetection of proteins expressed in the vesicles showed that both the motor protein kinesin and the gap junction protein Cx32 were present in the vesicle isolate. β-Tubulin and GAPDH were almost totally excluded from the vesicle isolate as expected for these cytosolic soluble proteins. *Arrows* and *labels* show the marker-correlated molecular weight migrations for each protein, which fall close to the reported migrations. An unspecific band below kinesin and above tubulin and GAPDH present in both tissue and vesicle samples, at 72 KDa (*small arrowheads*), is due to the secondary goat anti-mouse monoclonal antibody (see under "Results and supplemental Fig. 1").

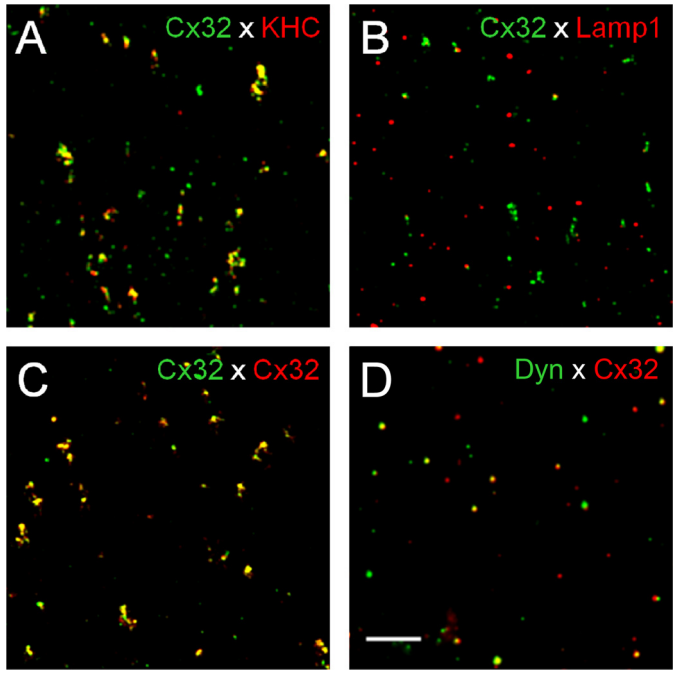

FIGURE 3. **Double immunoassaying of isolated vesicles.** Cx32 and kinesin co-localize in vesicles. Vesicle isolate was perfused into glass chambers, and double-antibody immunostaining was performed for Cx32 and several proteins of interest. Examples of results obtained are shown here, and analyzed data for degrees of co-localization are presented in Table 1. *A*, rabbit polyclonal anti-kinesin antibody (*red*, AKIN01) overlapped 36% with all Cx32-positive signals (*green*). Other kinesin antibodies did not exhibit such a high degree of co-labeling (Table 1). *B*, the late endosome/lysosomal protein, Lamp1 (*red*), poorly co-localized with Cx32 signal (*green*, 6.7%), suggesting that Cx32 in the vesicle isolate does not extensively reside in lysosomes. *C*, a positive control experiment using mouse monoclonal (*green*) and rabbit polyclonal (*red*) antibodies against Cx32 yielded high overlapping signals (*yellow*, 54.6%). *D*, an antibody against dynein light chain (*red*) also labeled a large portion of Cx32-positive vesicles (*green*, 32.8%).

are not bound to tubulin under these conditions. The presence of kinesin motor proteins in liver homogenate and vesicle isolate indicates that these vesicles likely contain the necessary molecular components for active protein trafficking. A more careful study of the protein composition of these vesicles has been previously published (19), demonstrating the presence of other trafficking markers in this vesicle fraction. We also noticed a 72-KDa band in all blots where a primary monoclonal antibody was used. Our control blot using a mouse monoclonal anti-synaptophysin (a neuronal marker) antibody on liver tissue and vesicle samples (supplemental Fig. 1) showed only a 72-KDa band, confirming this band as a nonspecific protein detected by the goat anti-mouse HRP-conjugated secondary antibody.

Immunolocalization of Cx32 and Kinesin in Vesicle Isolates—We next determined the fraction of Cx32-containing vesicles that co-localized with kinesin, which we expected would reflect the relative number of motility-competent Cx32-containing vesicles. We diffused vesicle isolate into a glass micro-chamber, and after allowing material to bind to the surface, we immunoassayed for Cx32 (Fig. 3) and kinesin (as well as for other proteins) and calculated the percentage of area co-localization of labeled vesicles, as well as a more quantitative Mander's coefficient (Table 1). Although several kinesin antibodies labeled varying proportions of Cx32-containing vesicles (*e.g.* kinesin antibody AKIN-01 labeled 36% of Cx32-containing vesicles), Cx32-positive vesicles were on average co-labeled 19% by all anti-kinesin antibodies. Labeling vesicles with two antibodies against Cx32 from different hosts (mouse and rabbit) resulted in 50–60% co-labeling. Interestingly, Cx32-containing vesicles were 33% labeled for dynein light chain, a component of the microtubule minus-end-directed dynein motor, indicating that a sizable percentage of these vesicles might also use dynein motor for trafficking. We observed that only 7% of Cx32-containing vesicles were co-labeled with lysosomal marker Lamp1, whereas 44% were co-labeled with the early endosome marker, EEA1. We interpreted these results to mean that the Cx32-containing vesicles in this pool represent material that has been endocytosed recently and not yet directed for lysosomal degradation. Rab4, another marker of a subset of early and recycling endosomes, only co-labeled 9% of the Cx32-containing vesicles, suggesting that Cx32-containing vesicles are not regulated by Rab4 or do not recycle. The finding that 63% of Cx32-labeled vesicles were co-labeled with clathrin suggests a strong dependence of this connexin protein for clathrin-mediated trafficking. The Cx32-containing vesicles also had 36% co-localization with Cx26, the other major liver gap junction protein, which could suggest co-transport of these two connexin proteins within the same vesicle. A conclusion from these antigen profiles is that in the vesicle isolate, a considerable fraction of the Cx32-positive

TABLE 1
Double immunocytochemistry of vesicles
Vesicles perfused in micro-chambers were double-immunolabeled and analyzed for Cx32 colocalization.

Cx32 against	% of colocalized area (±S.E.)	Mean Mander's coefficient[a]
Kinesin (01)	36.4% ± 4.1	0.49
Kinesin (H2)	11.3% ± 1.7	0.17
Kinesin (04)	10.7% ± 1.4	0.15
Kinesin light chain[a]	16.2% ± 7.7	0.49
Dynein light chain	32.8% ± 5.1	0.41
Rab4	9.4% ± 2.5	0.12
EEA1	44.4% ± 2.3	0.64
Lamp1	6.7% ± 2.6	0.08
Clathrin	62.5% ± 1.7	0.83
Cx26	36.0% ± 14.2	0.68
Cx32 (rabbit)	54.7% ± 10.2	0.6
Control:control	1.4%	

[a] See under "Experimental Procedures."

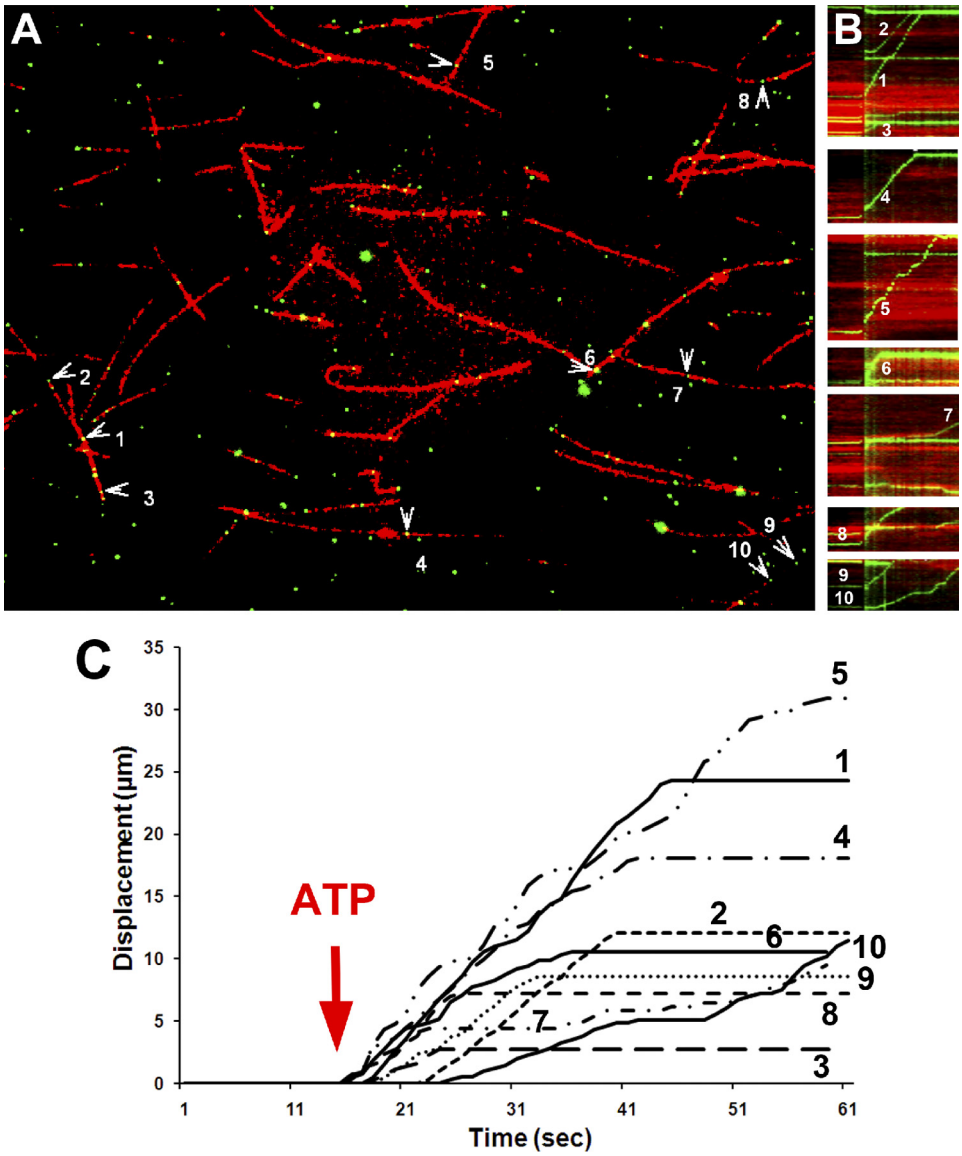

FIGURE 4. **Micro-chamber motility assays show ATP-dependent motility of Cx32-stained vesicles on fluorescently labeled microtubules.** Rhodamine-labeled microtubules were added to glass micro-chambers (see under "Experimental Procedures") followed by rat liver vesicle isolate and then indirectly fluorescently labeled with rabbit polyclonal anti-Cx32 antibody. *A*, an example of one experiment where 10 out of 94 vesicles were motile. Vesicle motility was recorded at 37 °C, before and after perfusion of 50 μM ATP. Differential interference contrast (not shown) and fluorescent images were taken at 1 Hz for 60 s. *Numbered arrowheads* show motile vesicles (see supplemental Movie 3). *B*, motility profile graph (kymographs) of all 10 numbered vesicles in *A*, showing the cumulative displacement *versus* time. Displacement is marked on the *y* axis, and time is marked on the *x* axis. The occurrence of "upward" but not "downward" displacement is indicative of unilateral vesicle movement along the microtubule. Note that the time of ATP addition is denoted by a *vertical green line*. Also note that some vesicles start later, pause more, or stop moving (*horizontal line*) earlier than others, showing the diverse motile nature of these vesicle. *C*, plot of cumulative displacement as a function of time obtained from manual tracking of vesicles shown in *A*. Due to unilateral displacement, these graphs look similar to the kymographs in *B*. *Numbers* correspond to vesicles in *A*.

vesicles are early endocytic and contain microtubule motors. These vesicles were then labeled with monospecific antibodies against Cx32 to study their behavior in an *in vitro* ATP-dependent motility assay on fluorescently labeled microtubules. We have also performed an immunoprecipitation assay to determine whether Cx32 and kinesin interact (supplemental Fig. 2). What we observed was the ability of Cx32 to pull down significant amounts of kinesin; however, immunoprecipitating kinesin led to a small yield of Cx32, which we interpret as a reflection of the relative proportions of associated protein.

Vesicle Motility—To study the motility inherent in these vesicles, we performed an *in vitro* motility assay in which we polymerized purified Paclitaxel-stabilized rhodamine-labeled microtubules (see under "Experimental Procedures") and flowed them into 5–10-μl volume glass chambers followed by aliquot of the vesicle isolate. We then performed a mini-immunostaining procedure using anti-Cx32 antibody and Alexa Fluor 488-labeled secondary antibody. This procedure resulted in many green-labeled particles attaching to red microtubules that were readily distinguished from one another (Fig. 4). On average, an image field of 150 × 115 μm yielded 80–200 vesicles resting on 50–80 microtubules, each ~20 μm in length. These values did not change dramatically under different conditions, except that bundling of microtubules occasionally

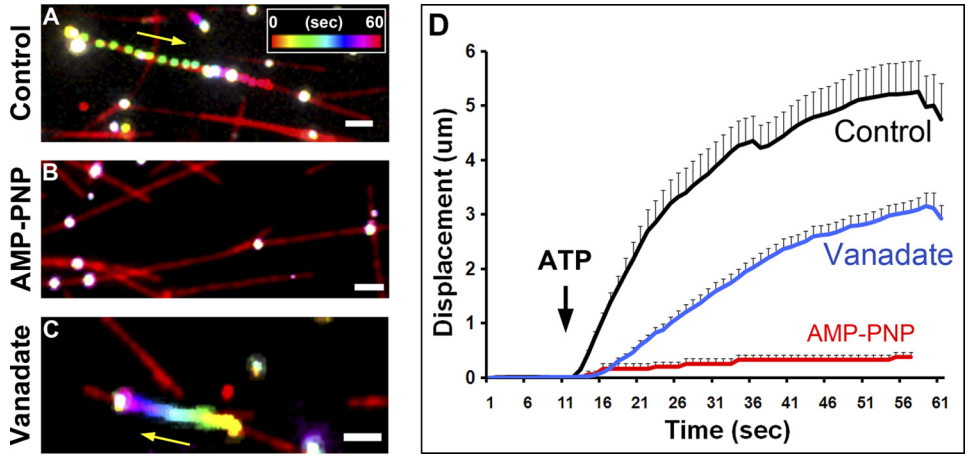

FIGURE 5. **Cx32-containing vesicle motility is sensitive to kinesin but not dynein inhibitors.** We applied AMP-PNP, a kinesin inhibitor, and vanadate, a dynein inhibitor to discriminate between the motor families involved in Cx32-containing vesicle motility. *A*, a representative, time- and color-coded figure shows the movement of a vesicle in control conditions with ATP. Note that spacing between vesicle movements is indicative of fast movements. The *inset* shows the color-time calibration bar. *B*, AMP-PNP abolished all movement upon ATP addition, and thus, vesicles are seen as *white*. *C*, although vesicle motility was still observed with vanadate incubation in a number of vesicles, less movement was observed. *D*, an averaged cumulative displacement graph for all three conditions shows that although vanadate maintains motility, there is an effect on the average final distance traveled by Cx32-containing vesicles. This in most cases is due to an increase in stationary dwell time and not a change in vesicle speed (see under "Results"). All conditions were normalized in time to the time of ATP addition (*black arrow*). AMP-PNP affected both the number of motile vesicles as well as speed (Fig. 6). Control ($n = 26$), AMP-PNP ($n = 5$), vanadate ($n = 32$). The *yellow arrow* highlights direction of vesicle movement. The *white bar* in *A–C* = 2 μm.

occurred in older microtubule samples, likely the result of deteriorated Paclitaxel, and most of these were discarded from analysis. Upon the addition of 50 μM ATP, we digitally recorded for 1 min and registered several vesicles gliding along microtubules (Fig. 4 and supplemental Movie 3). Occasionally, we observed vesicles that overtook other motile vesicles or collided with stationary vesicles and either continued moving or stopped all together. However, we did not observe clear events that were suggestive of either fusion or fission of vesicles. We also observed vesicles that would transfer from one microtubule to another (supplemental Movie 4). In some cases, the microtubules would detach from the glass and glide across glass-bound fluorescent vesicles (in these cases, we measured an average speed of microtubule gliding at 1.19 μm/s, with relatively few pauses), which made tracking motile vesicles on these microtubules difficult, and therefore, we removed them from analysis. Fig. 4*A* shows a model field of vesicles sampled in one experiment. The motility profiles of each of the tracked vesicles are shown in the pseudo-line graphs (Fig. 4*B*), where time is on the abscissa and the track length is on the ordinate. It is noticeable that the profiles of these vesicles demonstrate various behaviors, with variable stationary dwell times (slope = 0) but similar speeds (slope > 0) when in motion. We tracked these vesicles and obtained an average vesicle speed during motion of 0.59 ± 0.05 (S.E.) μm/s, the average distance traveled was 13.5 ± 2.7 μm, average stationary dwell time was 3.7 ± 2.2 s, and the average vesicle travel time was 22.1 ± 3.3 s. Out of the 94 vesicles attached to microtubules, 10 vesicles were motile, demonstrating that in this experiment, 10.6% of all vesicles in the field of view were able to travel along microtubules upon ATP stimulation. The results from 28 such experiments demonstrated that in control experiments, on average, six vesicles per field were motile, which accounted for 5.4% of all vesicles attached to microtubules. A total of 170 motile vesicles were studied in control conditions and showed average travel times of 13 s at an average vesicle speed of 0.44 ± 0.02 μm/s, close to the recorded speeds of kinesin-driven motility. The fluorescent areas of most motile vesicles were 4–9 pixels (corresponding to signals of 0.4–0.7 μm in diameter); however, we saw dimmer and smaller motile vesicles (1–2 pixels and only one or two vesicles per field), which we excluded from the analysis.

Inhibition of Motor Proteins—Plus-end motility is only driven by kinesin motor proteins (with the motor domains in the N terminus), whereas minus-end motility is largely driven by dynein and a minority of C-terminal motor kinesins (20). Although we did not label these microtubules for polarity, we never observed vesicles moving in opposite directions on the same microtubule. This observation thus suggests that Cx32-containing vesicle motility is due to only a plus-end kinesin or dynein and/or minus-end kinesin. To elucidate which family of motor proteins was involved in Cx32-labeled vesicle motility, we applied two general motor inhibitors: AMP-PNP, an analog of ATP that has been used to preferentially inhibit kinesin motors (21–23), and vanadate, an inhibitor of ATPases, which preferentially inhibits dynein motors at low concentration (24–26). When we added 50 μM ATP to our motility chambers in the presence of 1 mM AMP-PNP, we observed very little motility (Fig. 5*B* and supplemental Movie 5*B*), whereas motility was still observed in the presence of 5 μM vanadate (Fig. 5*C* and supplemental Movie 5*C*) or in control conditions (Fig. 5*D* and supplemental Movie 5*A*). Although vanadate slightly increased the number of motile vesicles (to 7.1%; no statistical difference, $p >$ 0.05), it did not significantly affect the average vesicle speed (0.37 μm/s ± 0.06) in comparison with controls. When we averaged the motility profiles of three experiments in each condition, it is clear that there was a subtle effect of vanadate on motility (Fig. 5*D*), with the total distance traveled by the vesicles at the end of the run shorter than in control conditions. The average distance traveled was 3.1 ± 0.2 (S.E.) μm in the presence of vanadate and 5.6 ± 1.1 μm in control conditions (Stu-

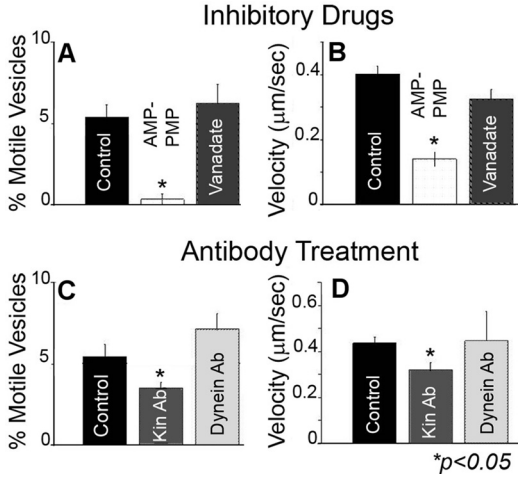

FIGURE 6. **Number and speed of Cx32-containing vesicles are sensitive to kinesin inhibitor and anti-kinesin antibody.** Summary data from vesicle motility experiments are shown. *A*, the average number of motile vesicles was not different from control conditions for vanadate; however, AMP-PNP nearly abolished vesicle motility (Student's *t* test, * = $p < 0.05$). Similarly, in *B*, the few remaining AMP-PNP-treated motile vesicles showed dramatically reduced average speeds ($p < 0.05$). Vanadate had no significant effect on the number of motile vesicles or speed. We tested whether anti-kinesin antibody would replicate the effects of AMP-PNP. *C*, incubation of vesicles with 100 μM anti-kinesin antibody (*Kin Ab*) (SUK4), prior to ATP addition, had a significant effect on the number of motile vesicles, in comparison with control conditions ($p < 0.05$). Like vanadate, anti-dynein antibody (*Dynein Ab*) had no significant effect on the percentage of motile vesicles. *D*, vesicle speed was likewise significantly affected by anti-kinesin antibody ($p < 0.05$). Vanadate had no significant effect. *Error bars* = S.E. All Student's *t* tests performed were two-sample, two-tailed. Control, $n = 28$ (170 motile vesicles analyzed); AMP-PNP, $n = 6$ (four motile vesicles); vanadate, $n = 5$ (70 motile vesicles); kinesin antibody, $n = 3$ (19 vesicles); dynein antibody, $n = 3$ (21 vesicles).

dent's *t* test $p < 0.05$). Upon further scrutiny, we discovered that the apparent drop in displacement was not due to a change in the average speed, but rather to increased frequency and duration of pauses during the movements. Thus, in control conditions, the average total vesicle pause duration (dwell time) was 6.6 ± 1.5 s, whereas in the presence of vanadate, vesicle dwell time was 16.8 ± 1.8 s, a 2.5-fold change that is significantly different (Student's *t* test, $p < 0.05$). Because the dwell time of control conditions was very similar to the average dwell time of 6 s previously reported for ATP-activated labeled kinesins on microtubules (27), the prolongation caused by vanadate may reflect an interaction between dynein and kinesin proteins that modifies processivity along microtubules. There was no significant difference between control and vanadate conditions for the delay of the onset of vesicle movement after ATP addition (not shown). The effects of the drugs AMP-PNP and vanadate on the number of motile vesicles and their velocity are summarized in Fig. 6, *A* and *B*.

To further evaluate the dependence of Cx32-labeled vesicular motility on functional motor proteins, we applied antibodies that interfere with kinesin function and compared the results with untreated controls and preparations treated with dynein antibody. As summarized in Fig. 6, *C* and *D*, results from experiments with blocking antibodies mimicked the results obtained with the inhibitory drugs (Fig. 6, *A* and *B*). The addition of anti-kinesin antibody significantly decreased the number of motile vesicles to around 3% ($p < 0.05$) but not to the extent that AMP-PNP did, whereas anti-dynein antibody increased slightly but not significantly to 7% (Fig. 6*C*). Vesicles that retained motility in the presence of anti-kinesin antibody were moderately, but significantly, slower than controls (Fig. 6*D*). Application of anti-dynein antibody had variable effects but did not differ significantly from control conditions.

DISCUSSION

The exogenous expression of fluorescently tagged gap junction proteins, in particular, Cx43, has clearly demonstrated that vesicles containing connexons are closely associated with microtubules and actin filaments and move linearly within cells (28). Moreover, cytoskeletal disrupting agents have been shown to interfere with normal connexin delivery to the plasma membrane (5, 6, 29). Such targeted delivery through cytoskeletal networks is likely to be especially important in polarized cells such as hepatocytes, where apical and basolateral membrane domains are segregated by tight junctions (30).

We have observed that in the hepatocyte cell line WIF-9B, vesicles containing exogenously expressed Cx32-GFP travel inside the cells through linear pathways toward the cell periphery, and this movement is disrupted by the microtubule-disorganizing drug nocodazole. To determine the characteristics of the movement of connexin-containing vesicles, including involvement of motor proteins, we have obtained a rat liver vesicle isolate that contains gap junction proteins and not only described the presence of cellular components of microtubule trafficking necessary for protein delivery to the surface (*i.e.* kinesin motors) but also reconstituted *in vitro* ATP-driven motility of these vesicles and characterized their behavior.

We determined that kinesin is a major player in the trafficking of these vesicles; however, we have not identified which specific kinesin isoform is involved in our assay. Although our Western blots were able to tell us the presence of kinesin and Cx32 in our vesicle preparations, the advantage of being able to perform immunochemistry directly on vesicles in the microchambers has allowed us to determine the co-localization of these two proteins within the same vesicle. Although we have focused on kinesin and Cx32 in this study, a more extensive characterization of proteins present in these vesicles was performed in Bananis *et al.* (19), including the presence of dynein in this vesicle pool, as well as several Rab proteins involved in vesicular trafficking. Although we have looked only at Rab4, which we see only as a small fraction in Cx32-containing vesicles, we do see a fair amount of dynein co-localization. We are unsure what the presence of a presumably inactive dynein (*i.e.* motility is unaffected by dynein inhibitor) means for the trafficking of these Cx32-containing vesicles. Immunostaining of these vesicles indicated that the isolated vesicle fraction is a diverse population, consisting of a high percentage of Cx32-positive vesicles that were largely early endosomal, as indicated by presence of EEA1, and showed overlap of staining with antibodies to both kinesin and dynein motor proteins, clathrin, and the other major hepatocyte gap junction protein, Cx26. Cx26 and Cx32 are known to oligomerize within the same cell and at apposing membranes, and although they are found well co-localized within vesicles, the lower percentage of co-labeled vesicles suggests that perhaps there is a minor level of sorting of these two connexins for vesicular transport, which may be due

to different exit sites (*i.e.* endoplasmic reticulum or Golgi network) during membrane delivery, as has been previously reported (31), or subunit discrimination during endocytosis. The latter may seem less probable, given the ability for these two connexins to intermix laterally once they are incorporated into the plasma membrane.

The large percentage of clathrin-positive vesicles containing Cx32 is an interesting and unexpected finding. Clathrin normally dissociates rapidly after endocytosis. We are currently investigating this observation; however, a plausible explanation for the large percentage of Cx32-containing vesicles associated with clathrin may be the rapid turnover rate that has been reported for Cx32. The higher endocytic rate would result in a higher proportion of Cx32-positive vesicles associated with clathrin. The high proportion of labeling of Cx32 to the early endocytic marker EEA1 is in agreement with this idea. Additionally, another contributor to the high clathrin content seen in these Cx32-containing vesicles might be vesicles en route to the plasma membrane that recently budded from endoplasmic reticulum or Golgi network, which we would expect to also be in high proportion. Interestingly, Lamp1, a lysosomal resident protein, was weakly present in Cx32-positive vesicles, suggesting that in our low density vesicle preparations, lysosomes containing Cx32 are not abundant. This may be due to the degradation pathway of Cx32 involving proteasomes (32) or the methodology applied, which enriches low density fractions and excludes high density particles, such as the internalized double-membraned annular junctions.

Our live micro-chamber experiments demonstrated that Cx32-containing vesicles from liver bound to microtubules and that, upon ATP stimulation, roughly 5% of all Cx32-labeled vesicles that were attached to microtubules were motile. Although we attribute the low number of motile vesicles to the detrimental effects on kinesin function of the isolation of low density vesicles, it is also possible that the low percentage represents the total pool of actively motile vesicles in hepatocytes. The average speed of these vesicles is well within that expected for kinesin motors working *in vitro* under load (21, 33) and those reported by connexin-labeled vesicles in live imaging of cells (8). We also observed that the motile vesicles *in vitro* were sensitive to AMP-PNP and not vanadate, suggesting that the motility is driven by kinesin, and not dynein, which has more rapid motility (25, 26). Together with our immunoprecipitation of kinesin with Cx32 antibodies (supplemental Fig. 2), these data suggest a strong interaction between these two proteins.

From the moderate proportion of Cx32-positive vesicles that co-labeled with dynein, we would have expected some dynein-dependent motility in these vesicles. The lack of inhibition of dynein motility by vanadate suggests that the Cx32-containing population of this vesicle isolate contains very few active dynein motor proteins. Dynein is believed to play a major role in endocytosis and delivery to lysosomal compartments. Most studies looking at the endocytosis of gap junctions (34–36) have demonstrated that gap junction proteins are internalized as double bilayer vesicles called annular junctions. We believe that this compartment would not be found in our low density vesicle isolate because of their heavier density and may be the reason for no dynein activity. Therefore, perhaps our isolated pool of vesicles contains hemichannels (connexons) in single bilayers that have been internalized from non-junctional membranes in the rat liver and are early endosomes with inactive dynein motor proteins or exocytic vesicles carrying inactive dynein to the surface. The interesting observation that inhibition of dynein with vanadate slightly increased vesicle motility has to be further explored to see whether the cause is due to a loss of a tug-of-war situation between dynein and kinesin.

In our fluorescently tagged connexin exogenous expression experiments in WIF-B9 cells, we observed a large range of particle sizes, including some of which were large and motile, which could be representative of non-junctional endocytic vesicles or annular junctions, although we clearly observed the latter a day or two later than when these experiments were carried out. Particles ranged in fluorescent signal areas from 0.02 to 0.6 μm^2, with an average of 0.2 $\pm$ 0.02 μm^2. The larger particles might belong to endocytosed Cx32 and thus may traffic in a different manner to those in the exocytic pathway. We therefore determined whether there was any correlation between size and speed of particles. What we find is a small trend toward a negative correlation between particle area and maximum speed (with particles with areas >0.5 μm^2 having maximum speeds <0.05 $\mu m/s$); however, both parameters are subject to high variability, and thus, the relationship is not statistically significant (correlation -0.24; regression -0.23; both $p > 0.05$). We also did not observe a clear distinction in speeds, which would have been expected for different particle pathways (graphs not shown).

Our conclusion is that the motility seen in the Cx32-stained vesicles isolated with this protocol is dependent on kinesin motor function. We would further speculate that the motile fraction of vesicles from our isolate pool is composed of low density vesicles destined for delivery to the plasma membrane, although we require further experiments to verify this postulate. We believe that the association of kinesin with Cx32 in relation to protein trafficking adds another level of regulation to Cx32 function and needs to be further investigated.

Acknowledgments—We are grateful for advice and assistance of Drs. Anne Muesch, Sangeeta Nath, Souvik Sarkar, Sylvia Suadicani, Carmen E. Flores, Mia Thi, and Heather Duffy and Marcia Urban-Maldonado, Frances Andrade, and the late Joe Zavilowitz.

REFERENCES

1. Falk, M. M., Kumar, N. M., and Gilula, N. B. (1994) *J. Cell Biol.* **127,** 343–355
2. Musil, L. S., and Goodenough, D. A. (1993) *Cell* **74,** 1065–1077
3. Falk, M. M., Buehler, L. K., Kumar, N. M., and Gilula, N. B. (1997) *EMBO. J.* **16,** 2703–2716
4. Maza, J., Das Sarma, J., and Koval, M. (2005) *J. Biol. Chem.* **280,** 21115–21121
5. Segretain, D., and Falk, M. M. (2004) *Biochim. Biophys. Acta* **1662,** 3–21
6. Laird, D. W. (2006) *Biochem. J.* **394,** 527–543
7. Paulson, A. F., Lampe, P. D., Meyer, R. A., TenBroek, E., Atkinson, M. M., Walseth, T. F., and Johnson, R. G. (2000) *J. Cell Sci.* **113,** 3037–3049
8. Lauf, U., Giepmans, B. N., Lopez, P., Braconnot, S., Chen, S. C., and Falk, M. M. (2002) *Proc. Natl. Acad. Sci. U.S.A.* **99,** 10446–10451
9. Johnson, R. G., Meyer, R. A., Li, X. R., Preus, D. M., Tan, L., Grunenwald, H., Paulson, A. F., Laird, D. W., and Sheridan, J. D. (2002) *Exp. Cell Res.* **275,** 67–80

10. George, C. H., Kendall, J. M., and Evans, W. H. (1999) *J. Biol. Chem.* **274,** 8678–8685
11. Meller, K. (1981) *Anat. Embryol.* **163,** 321–330
12. Wang, Y., and Rose, B. (1995) *J. Cell Sci.* **108,** 3501–3508
13. Theiss, C., and Meller, K. (2002) *Exp. Cell Res.* **281,** 197–204
14. Guo, Y., Martinez-Williams, C., and Rannels, D. (2004) *Chest* **125,** 110S
15. Giessmann, D., Theiss, C., Breipohl, W., and Meller, K. (2005) *Anat. Embryol.* **209,** 391–400
16. Murray, J. W., Bananis, E., and Wolkoff, A. W. (2000) *Mol. Biol. Cell* **11,** 419–433
17. Murray, J. W., Bananis, E., and Wolkoff, A. W. (2002) *Anal. Biochem.* **305,** 55–67
18. Manders, M. M., Verbeek, F. J., and Aten, J. A. (1993) *J. Microsc.* **169,** 375–382
19. Bananis, E., Nath, S., Gordon, K., Satir, P., Stockert, R. J., Murray, J. W., and Wolkoff, A. W. (2004) *Mol. Biol. Cell* **15,** 3688–3697
20. Hirokawa, N., Noda, Y., and Okada, Y. (1998) *Curr. Opin. Cell Biol.* **10,** 60–73
21. Brady, S. T., Pfister, K. K., and Bloom, G. S. (1990) *Proc. Natl. Acad. Sci. U.S.A.* **87,** 1061–1065
22. Leopold, P. L., McDowall, A. W., Pfister, K. K., Bloom, G. S., and Brady, S. T. (1992) *Cell Motil. Cytoskeleton* **23,** 19–33
23. Lasek, R. J., and Brady, S. T. (1985) *Nature* **316,** 645–647
24. Kobayashi, T., Martensen, T., Nath, J., and Flavin, M. (1978) *Biochem. Biophys. Res. Commun.* **81,** 1313–1318
25. Brady, S. T. (1991) *Neuron* **7,** 521–533
26. Harrison, R. E., and Huebner, E. (1997) *Cell Motil. Cytoskeleton* **36,** 355–362
27. Seitz, A., and Surrey, T. (2006) *EMBO. J.* **25,** 267–277
28. Piehl, M., Lehmann, C., Gumpert, A., Denizot, J. P., Segretain, D., and Falk, M. M. (2007) *Mol. Biol. Cell* **18,** 337–347
29. Olk, S., Zoidl, G., and Dermietzel, R. (2009) *Cell Motil. Cytoskeleton* **66,** 1000–1016
30. Kojima, T., Murata, M., Yamamoto, T., Lan, M., Imamura, M., Son, S., Takano, K., Yamaguchi, H., Ito, T., Tanaka, S., Chiba, H., Hirata, K., and Sawada, N. (2009) *Histol. Histopathol.* **24,** 1463–1472
31. Martin, P. E., Blundell, G., Ahmad, S., Errington, R. J., and Evans, W. H. (2001) *J. Cell Sci.* **114,** 3845–3855
32. Goodenough, D. A., and Paul, D. L. (2009) *Cold Spring Harb. Perspect. Biol.* **1,** a002576
33. Howard, J., Hudspeth, A. J., and Vale, R. D. (1989) *Nature* **342,** 154–158
34. Youson, J. H., Peek, W. D., and Shivers, R. R. (1983) *Anat. Embryol.* **167,** 379–389
35. Jordan, K., Chodock, R., Hand, A. R., and Laird, D. W. (2001) *J. Cell Sci.* **114,** 763–773
36. Leithe, E., Brech, A., and Rivedal, E. (2006) *Biochem. J.* **393,** 59–67